16th World Conference on Earthquake, 16WCEE 2017
Santiago Chile, January 9th to 13th 2017
Paper N° 3009
Registration Code: S-N1464321005

EXPERIMENTAL CYCLIC RESPONSE OF RC COLUMNS WITH DEBONDED LONGITUDINAL REINFORCEMENT IN THE PLASTIC HINGE REGION

M. T. Nikoukalam(1), P. Sideris(2)

(1) *Ph.D. Candidate, Dept. of Civil, Environ. and Archit. Engineering, University of Colorado – Boulder, mt.nikoukalam@colorado.edu*
(2) Assistant Professor, Dept. of Civil, Environ. and Archit. Engineering, University of Colorado – Boulder, petros.sideris@colorado.edu

Abstract

This paper discusses the findings of an experimental study investigating the response of nearly full-scale (~1:1.14) reinforced concrete (RC) columns incorporating partially debonded longitudinal reinforcement in the location of the plastic hinge as a means of improving the ductility capacity of RC columns and RC moment resisting frames. Early fracture of longitudinal reinforcement due to strain concentrations in locations of high moment demands and early concrete crushing due to bond stress effects cause rapid strength and stiffness degradation limiting the ductility capacity of RC columns in buildings and bridges. In this study, the concept of partial debonding of the longitudinal reinforcement at the column ends (i.e., locations of high moment demands) as a means of spreading locally induced deformations over larger rebar lengths is investigated. Spreading local deformations over larger rebar lengths results in smaller peak rebar strains delaying rebar fracture. The efficiency of the proposed concept is quantified through quasi-static cyclic testing of three nearly full-scale cantilever columns. All columns have a 14” × 14” [356 mm × 356 mm] square cross-section and shear span-to-depth ratio of 5.5. The first column has fully bonded reinforcement and serves as the reference column, while the second and the third columns have partially debonded reinforcement at their bottom end over half of the plastic hinge length and the entire plastic hinge length, respectively. The reference column was part of a four-bay three-story RC building designed as special moment resisting frame, per ACI 318-14. All specimens were subjected to a constant vertical load that provided an axial force ratio of 20%, and lateral displacement-controlled cyclic loading of progressively increasing amplitude until complete loss of the vertical load carrying capacity. Based on the experimental data, partial debonding was proven to be effective in decreasing the extent of concrete damage to half of the plastic hinge length, as opposed to the full plastic hinge length for bonded reinforcement. Debonding alleviated strain localizations in the steel reinforcement, at least, for drift ratios below 2%. The peak lateral strength and stiffness decreased with the debonded length.

To facilitate further investigation of the proposed concept, three-dimensional finite element models of the column with the fully bonded reinforcement was generated using the ABAQUS general purpose finite element software. The computed response was in good agreement with the test data, providing the means of further assessing the efficiency of the proposed concept in moment resisting frames and other structures.

Keywords: Reinforced concrete column; large-scale testing; debonded rebar; finite element modeling; cyclic response

1. Introduction

One of the main sources of damage in reinforced concrete (RC) columns in both bridges and buildings is strain concentration in steel bars due to the bond between the longitudinal bars and the concrete that results to premature bar fracture. One of the methods used to alleviate the strain concentration in steel bars is partial debonding of the longitudinal bars from the surrounding concrete.

Partial dedonding has been extensively considered in precast concrete (PC) buildings and PC bridge columns. Nakaki et al. [1] employed the debonding technique in the beams of a precast/prestressed RC frame to prevent premature rebar fracture. The top and bottom reinforcement of the beams was grouted into sleeves and debonded for a specified length so that it can yield alternately in tension and compression without fracture. The results of the simulated seismic loading test showed that the sleeved debonded connection provide a significant energy dissipation capacity by eliminating the possibility of the premature rebar fracture. Trono et al. [2] employed debonded rebars to provide hysteretic energy dissipation in a damage-resistant recentering bridge column system containing hybrid fiber-reinforced concrete (HYFRC) and high-strength posttensioned steel strands. Based on the test results, the debonded bars provided hysteretic energy dissipation via significant yielding as they were designed, with lower strains compared to the conventional column. Pang et al. [3] used the debonding technique in a new beam-to-column connection to accelerate the construction of PC bridge bents in regions with high seismicity. They debonded a portion of the grouted length of longitudinal bars in the cap beam with the main purpose of reducing the local strain and prevent premature bar fracture by spreading the deformation along the debonded length. However, the cyclic lateral load tests showed that debonding of the longitudinal bars in the cap beam had little effect on the hysteretic performance of the system, while slightly reduced the lateral stiffness at low drifts. It was also observed that debonding of the longitudinal bars did not affect the buckling or fracture of these bars, since rather than uniaxial extension and compression of the bars under cyclic loads, fracture was occurred due to local low-cycle fatigue in flexure caused by buckling and straightening of the bar in the column region, away from the debonded region in the cap beam. Ou et al. [4] could successfully delay the fracture of the energy dissipation (ED) bars and increase the energy dissipation of precast segmental concrete bridge columns by partially debonding the ED bars, while the lateral strength was slightly decreased.

To enhance the seismic performance (particularly ductility and energy dissipation capacity) of precast concrete (PC) walls, Kang et al. [5] employed the method of debonded longitudinal bars with partially reduced cross sectional area at the plastic hinge zone of emulative PC walls to prevent early fracture of rebars and early concrete crushing caused by bond stress. The results of the cyclic loading tests showed that the overall deformation of the wall was governed by the deformation of the debonded rebars with significant reduction in concrete crushing.

Partial reinforcement debonding has also been considered in cast-in-place RC bridge and building systems. Kawashima et al. [6] studied the effect of debonding the main reinforcements at the plastic hinge region of the bridge columns, where main reinforcements were fully or partially debonded. From a cyclic loading test, they showed that debonding results in a dominant rocking response of the column with much less failure of concrete, and reduces the axial strain concentration in the longitudinal bars since the strain is averaged in the debonded length. They also showed that debonding slightly increases the ductility factor and reduces the lateral stiffness and energy dissipation. Aviram et al. [7] conducted an experimental and analytical study on circular column specimens representing cantilever bridge piers constructed with high-performance fiber-reinforced concrete (HPFRC). The HPFRC column-foundation interface of the test specimens was strengthened with dowel reinforcement to force most of the inelastic deformations to occur within the HPFRC column. They devised different debonding schemes to minimize damage localization by preventing large strain concentration and premature reinforcing bar fracture at the section where the dowel reinforcement was terminated. They showed that debonding of the dowel reinforcement is very effective in spreading of bar yielding along the column height and formation of several flexural cracks in the plastic hinge region. Pandey et al. [8, 9] proposed the debonding of longitudinal bars as an alternative way of enhancing the seismic performance of RC bridge columns with low shear reinforcement rather than just relying on increasing the shear reinforcement. They performed an extensive experimental study on a total of 15 RC columns by varying the bonding condition between the longitudinal reinforcement and concrete (perfect bonding, perfect debonding, and poor bonding), number of debonded longitudinal bars (mixed bond condition), the length of the debonded region, the shear span-depth ratio, and the ratio of shear strength to flexural strength, while all of the specimens with perfect bond conditions were purposely designed to fail in shear. The reversed cyclic test results showed that, both perfect and poor debonding of the longitudinal bars can completely change the failure mode of RC column from shear to flexure followed by a remarkable increase in the ductility up to 365%. They also showed that despite the great improvement in shear strength and ductility, specimens with poor bond and perfect debonding conditions provide lower energy dissipation capacity compared to an ordinary RC column. This is attributed to the occurrence of wide flexural cracks in the column-footing joint. The results also showed large differences in the magnitude of the axial strain in the height of the column with perfect bond, due to strain concentration near the column footing joint. However, in the specimens with the perfectly debonded reinforcement, the strain was averaged out over the entire debonded length.

In cast-in-place RC building frames, Yu et al. [10] suggested partially debonding bottom reinforcing bars in the joint region of RC frames as a special detail to improve the structural resistance against progressive collapse under a column removal scenario. Based on the experimental quasi-static responses of the four RC frame specimens, the strain concentration was avoided in debonded bars and the strain was distributed uniformly prior to yielding, resulted in a significant increase in the fixed-end rotation at the middle joint interface by fully using the ductility capacity of the steel rebars.

Apart from bridge columns and beams in frame structures, Choi et al. [11] suggested the debonding technique to improve the ductility of the slab-column connections. Experimental investigations showed that partially debonding of the flexural reinforcement of the slab in the vicinity of the slab-column joint results to reduced strain concentration in the bars, reduced accumulated damage in the concrete, and improved drift capacity.

All the prior studies primarily focus on the effect of partial debonding of the longitudinal reinforcement on the behavior of PC and cast-in-place RC bridge columns, beam-column joint in frames under gravity load, and RC shear walls. The primary objective of this study is to investigate the effect of partial debonding of the longitudinal reinforcements in the plastic hinge of RC columns in special moment resisting frames designed for seismic regions based on ACI318-11. The efficiency of the proposed concept is quantified through quasi-static cyclic testing of three nearly full-scale cantilever columns with 14” × 14” [356 mm × 356 mm] square cross-section and shear span-to-depth ratio of 5.5. The performance of all specimens is assessed in terms of peak strength, lateral stiffness, ductility capacity, and damage pattern. . Moreover, to provide the means for further investigation of the proposed concept, a 3D finite element model of a column with fully bonded reinforcement is created in ABAQUS [12] and validated using data from the test.

2. Experimental program

2.1. Test specimens and test setup details

In order to assess the effect of partial debonding of the longitudinal reinforcements on the seismic behavior of RC columns with well-confined plastic hinge regions, three nearly full scale specimens were tested under reversed quasi-static cyclic loading. The prototype is the first floor column of a four-story four-bay special moment resisting reinforced concrete frame located in Burlington, Vermont [13]. Each bay is 19.6 ft (235 in.) [5.97 m] long, while each story is 12.1 ft (145 in.) [3.68 m] high. The first floor column has a cross section of 16 × 16 in^2 [406 × 406 mm^2]. The column was designed using ASCE/SEI 7-10 [14] and ACI 318-11 [15].

Similitude analysis was performed to meet testing capabilities of the Structures and Materials Testing Laboratory (STML) at the University of Colorado (CU) – Boulder. The selected length scale factor was 1.14. Fig. 1 (a) shows the dimensions and the reinforcement details of the test specimens. All specimens have a 14 × 14 in^2 [356 × 356 mm^2] cross-section while the distance between the lateral loading point and the column-to-footing joint was 77 in. [1.96 m], leading to a shear span-to-depth ratio of 5.5. Identical longitudinal reinforcement of 12 #6 [diameter = 0.75 in. [19 mm]] bars with a nominal yield stress of 60 ksi [414 MPa] were used for all specimens, resulting in a steel ratio of 2.7%. The transverse reinforcement was #3 [diameter = 0.375

in. [9.5 mm]] square ties at 3.5 in. [89 mm] spacing to provide shear capacity as well as confinement of the concrete. Based on ACI318-11 [15], additional confinement reinforcement shall be provided over a length l_o at the column end where flexural yielding is likely to occur as a result of inelastic lateral displacements of the frame. The length l_o was computed to be 15.5 in. [394 mm]. Where a column frames into a strong foundation element or wall, such that column yielding is likely under design earthquake loading, it is recommended by ACI318-11 [15] that the length of the confinement zone be increased to $1.5l_0$. Accordingly, additional confinement reinforcement is provided in a length of 23 in. ($1.5l_o$ = 23 in. [584 mm]) from the column-footing interface by reducing the spacing of the rectangular hoop reinforcement to 2.5 in. [64 mm] and providing two additional cross ties with #3 bars (Fig. 1(a)). The nominal yield stress of all transverse reinforcement bars was 60 ksi [414 MPa]. The concrete had normal density and specified compressive strength of 5.0 ksi [34.5 MPa].

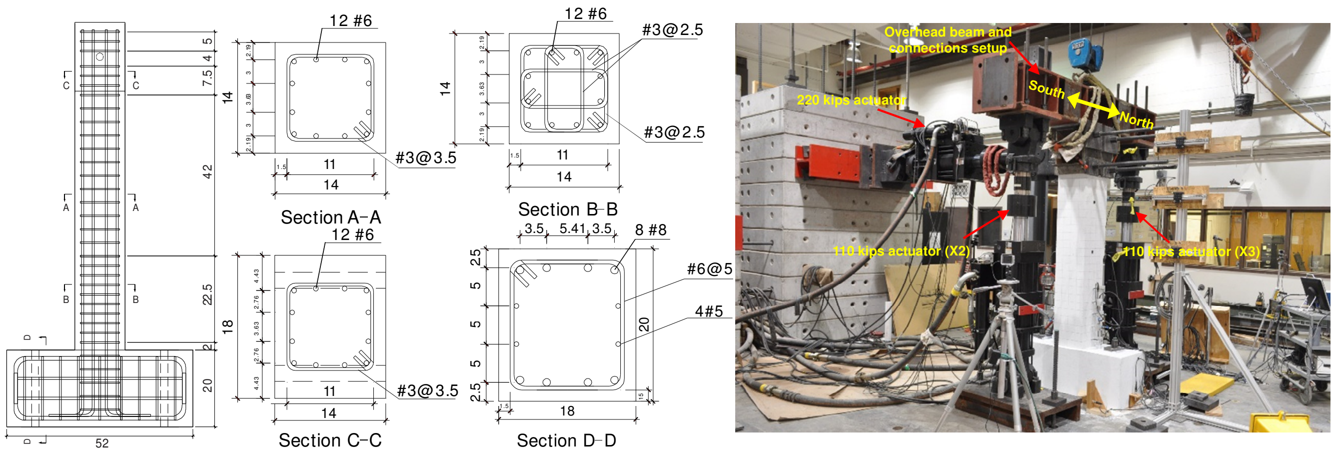

(a) (b)

Fig. 1 – (a) Details of test specimen; (b) details of the test setup (All dimensions are in inches [1 in. = 25.4 mm]).

Fig. 2 shows the debonded length in all specimens along with the details of the method used to debond longitudinal reinforcement from the concrete. Debonding of the longitudinal reinforcement was achieved using PVC pipes with inner diameter and thickness of 7/8 in. [22.2 mm] and 1/16 in. [1.6 mm], respectively. The PVC pipes were flexible enough so that they could bend with the reinforcing bars. The inside surface of the pipes was lubricated to remove the friction between the bar and pipe introduced by the tightness of pipes. The debonded length of the rebars was equal to 13 in. [330 mm] and 28 in. [711 mm] in partially (PDC) and fully (FDC) debonded column, respectively, out of which, 2 in. [51 mm] extended into the footing (Fig. 2). The pipes were placed on longitudinal bars and the location was properly fixed before casting of the concrete. Both ends of the pipe were water sealed using silicone gel.

Fig. 1 (b) shows the test setup of the columns tested. The specimen was anchored to the strong floor with two pre-stressed bars. The target gravity load from the design was 206 kips, i.e. equivalent to $0.2 f'_c A_g$, where f'_c is the nominal concrete strength of 5 ksi [34.5 MPa], and A_g is the gross cross sectional area of the column. The gravity load was applied by two (MTS) hydraulic actuators (X2 and X3) connected to the flanges of a stiff overhead beam bolted to the top of the column. To avoid any instability due to uneven action (movement/vertical displacement) of the two vertical actuators, force signal was sent to one actuator (X3 as master), while the other actuator (X2) was slaved to follow the displacement of the master. Reversed cyclic displacement-controlled lateral load was applied by an MTS hydraulic actuator (X1) at one end anchored to the column at the height of 77 in. [1.96 m] from the footing.

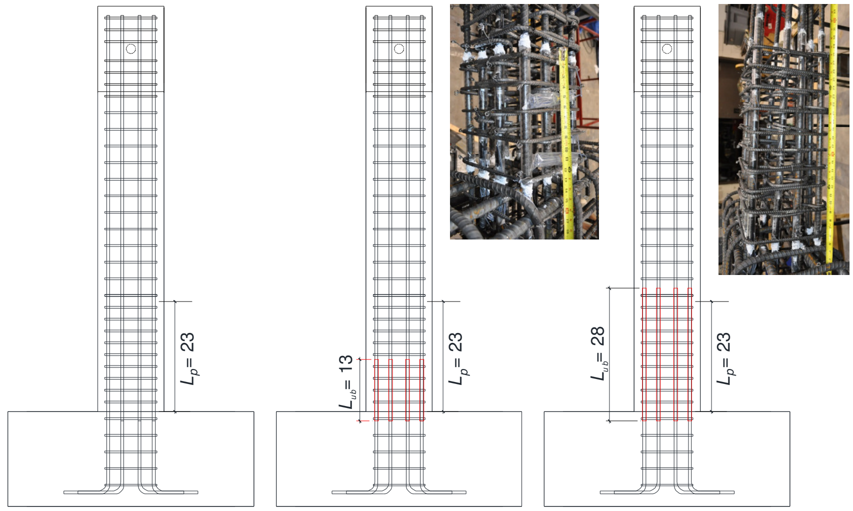

(a) (b) (c)

Fig. 2 – Length of the debonded region and details of debonding: (a) BC column, (b) PDC column, and (c) FDB column (All dimensions are in inches [1 in. = 25.4 mm]).

2.2. Instrumentation and loading protocol

Strain gauges were used to measure strains at several locations of longitudinal and transverse bars (Fig. 3(a)). The strain gauges layout (Fig. 3(e)) was identical in all specimens. Five longitudinal bars were equipped with strain gauges over the expected length of the plastic hinge above the column-to-footing interface, as shown in Fig. 3(e). Two gauges were placed 3.25 in. [83 mm] below the interface to monitor the axial strain in longitudinal bars within the footing. Strain gauges were placed in pairs for redundancy where the maximum change in the strain profile was expected (cross-section L6, Fig. 3(e)). Two gauges were placed on transverse bars at three locations (2 in. [51 mm], 9.5 in. [241 mm], and 17in. [432 mm] above the interface) over the expected plastic hinge length, indicated as S2 in Fig. 3(e).

A curvature rod system consisting of five linear voltage displacement transducers (LVDTs) on two sides of the column was used to measure relative rotations/curvatures over the expected length of the plastic hinge (~24 in. [610 mm] from the footing) (Fig. 3(b)). Two vertical LVTDs were connected to the west and east side of the footing to measure potential uplift, and two LVDTs were connected horizontally on north and south side of the footing to measure potential sliding of the specimen (Fig. 3(d)). Horizontal displacements were measured using three encoders over the height of the column, including the location of the applied lateral load, as shown in Fig. 3(c). Encoders were attached to a supporting reference frame that was fixed on the strong floor.

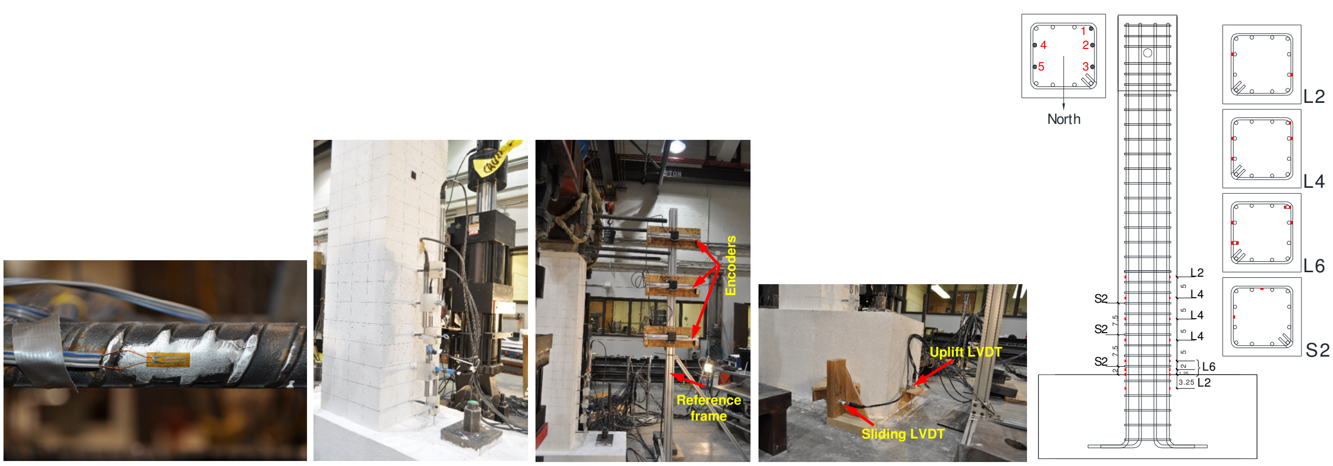

(a) (b) (c) (d) (e)

Fig. 3 – (a) Strain gauge on longitudinal reinforcement; (b) Curvature rod system (LVDTs); (c) Encoders; (d) Sliding and uplift LVDTs; (e) Strain gauges layout.

The test procedure was identical for all the specimens. First, an axial load of 206 kips [916 kN] was applied by the vertical actuators (X2 and X3). The axial load was monitored and controlled to remain constant during the test. Displacement-controlled reversed cyclic loading was subsequently applied with the loading protocol as shown in Fig. 4. The loading protocol consisted of symmetric cycles of increasing amplitude up to the maximum stroke of the horizontal actuator (X1) which was 12.6 in. [320 mm] (6.3 in. [160 mm] in each direction). Each set included two cycles with the same amplitude. Displacement amplitudes of 0.135%, 0.25%, 0.375%, 0.5%, 0.75%, 1%, 2%, 3%, 4.5%, 6.5%, and 8.26% drift ratios were applied, where drift ratio is defined as the ratio of the lateral displacement of the loading point to the loading height of the column (77 in. [1.96 m]). The loading was applied at a rate of 0.01 to 0.05 in./sec [0.25 to 1.27 mm/sec]. After reaching the maximum stroke of the horizontal actuator (X1), the actuator was contracted by 5 in. [127 mm] and extension washers were added between the actuator's swivel and the specimen. After extension, asymmetric cycle pairs with amplitudes of 10.5%, 12.5%, 14.5%, and 16 % in one direction and 0.5% in the other direction were applied at a rate of 0.05 to 0.08 in./sec [1.27 to 2 mm/sec].

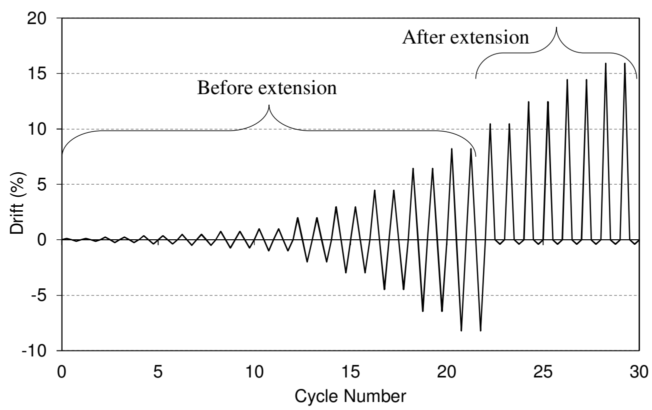

Fig. 4 – Test loading protocol

2.3. Test results

2.3.1. Experimental observations and hysteretic response

Force vs. displacement drift ratio relationships and envelope curves obtained from the forces and displacement drift ratios at the positive and negative peak amplitudes of each cycle are shown in Fig. 5. Forces have been corrected for the lateral contribution of the vertical actuators in the deformed configuration. It is observed that peak strength and unloading/reloading stiffness decreased with the debonded length, particularly at larger drift ratios. The elastic stiffness slightly decreased with the debonded length (see Table 1). Moreover, stiffness and force degradation increased with the debonded length (Fig. 5(a)). Softening, indicated by the negative slope of the post-peak branch of the force-displacement drift ratio curve (Fig. 5(b)), increased with the debonded length. Although debonding delayed rebar yielding, the deformation capabilities of the PDC and FDC specimens decreased (Fig. 5(b)), because the selected method of debonding did not restrain local rebar buckling, which was significant under the selected cyclic loading protocol.

Table 1 – Summary of test results (1 kip = 4.45 kN, 1 in. = 25.4 mm)

	BC	PDC	FDC
Elastic Stiffness, *E* (kips/in.)	77 [1]	71 [0.92]	68 [0.88]
Positive Peak Strength, F^{+}_{max} (kips)	32.4 [1]	30.6 [0.94]	28.4 [0.88]
Negative Peak Strength, F^{-}_{max} (kips)	-31.20 [1]	-32.3 [1.04]	-30.2 [0.97]

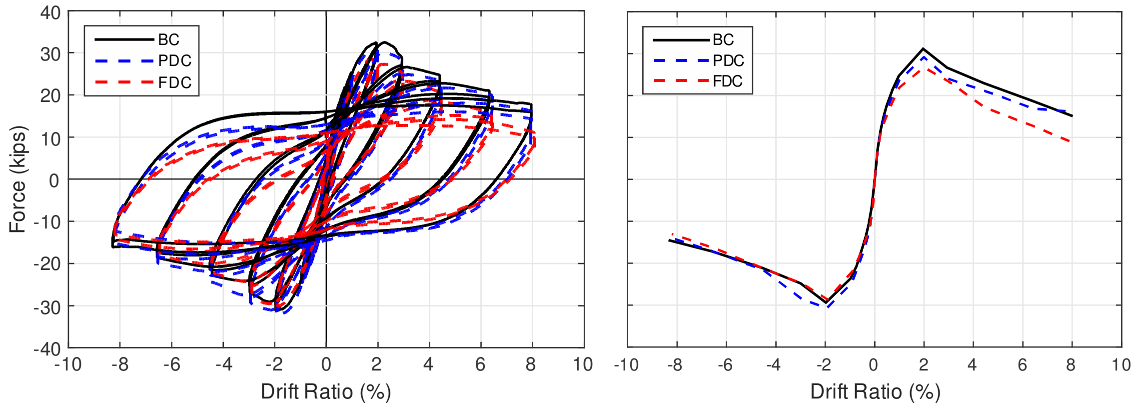

(a) (b)

Fig. 5 – (a) Force vs. displacement drift ratio hysteresis curves; (b) Force versus displacement drift ratio envelopes (before addition of extension washers) (1 kip = 4.45 kN)

The damage pattern for all the specimens at various drift ratios is compared in Fig. 6. Flexural cracks initiated at the column-to-footing joint at a drift ratio of 0.75% for the BC specimen and 0.5% for the PDC and FDC specimens, and propagated upwards with the displacement amplitude. Spalling was first observed at a 2% drift ratio, in all specimens, and increased with the displacement amplitude. For up to 8.26% drift ratio (i.e., before adding the extension washers), the damage to all specimens was, initially, in the form of concrete spalling and crushing, and was, subsequently, followed by yielding of the longitudinal bars. According to Fig. 6, it can be observed that the extent of concrete damage reduced with the debonded length. Specifically, for the BC specimen, concrete damage was observed over the entire (nominal) plastic hinge length (L_p = 23 in. [584 mm]), whereas, for the PDC and FDC specimens, the concrete damage did not exceed 12 in. [305 mm] from the bottom joint, even for a 14.5% drift ratio. This is attributed to the fact that the concrete can deform independent of the rebar and does not have to undergo the same strains as the reinforcement; thereby, localized concrete strains could not be spread over the plastic hinge length. Another important observation was that as the debonded length increased, the deformation mechanism of the column changed from flexural behavior to a rocking response at an interface slightly above the footing. The rocking response was mostly observed in the FDC specimen, for which the rocking interface was located approximately 3 in. [76 mm] above the column-to-footing joint.

After adding the extension washers, tests were conducted until four longitudinal bars and, at least, one bar at each side fractured. Fractures of the longitudinal bars of all column specimens are shown in Fig. 7. For the BC specimen, the first two rebar fractures occurred in the tension side during the third cycle at the peak drift ratio of 16% with 0.4 in/sec [10.2 mm/sec] loading rate. The other two bars in the tension side fractured during the fifth cycle at a drift ratio of 16% and loading rate of 0.4 in/sec. The test stopped after the fracture of one rebar in the compression side during the seventh cycle at 16% drift ratio with 0.8 in/sec loading rate. For the PDC specimen, first rebar fracture occurred in the compression side in the first cycle at 14.5% drift ratio. Three rebars in the tension side fractured during the second cycle at 14.5% drift ratio, while fracture of two bars in the compression side occurred during the second cycle at 16% drift ratio with 0.1 in/sec loading rate. For the FDC specimen, the first rebar fracture was observed in the compression side during the third cycle at the peak drift ratio of 16%. Three more bars fractured in the compression side during the fifth and sixth cycle at the 16% drift ratio and 0.4 in/sec [10.2 mm/sec] loading rate. The first rebar fracture in the tension side occurred during loading in the tenth cycle at 16% drift ratio and a loading rate of 0.8 in/sec [20.3 mm/sec] Two more fractures in the tension side occurred during the 12th cycle (16% drift ratio and 0.8 in/sec [20.3 mm/sec] loading rate), while the last rebar fractured during the 16th cycle at the same drift ratio and loading rate.

Visual inspection of all specimens at the end of each set of cycles concluded that all rebar fractures were caused by rebar buckling at the bottom of the columns. The longitudinal rebar buckled under compression at almost the same drift ratio (14.5 %) for all specimens over the free length (3.5 in. [89 mm]) between the first square tie above and below the column-to-footing interface. The cyclic loading resulted in large localized bending stresses that eventually caused low-cycle fatigue fracture without any observable necking in the rebar. Although partial debonding alleviated stress concentration in the steel rebar (as demonstrated below) before buckling occurred, it did not provide any additional resistance against local rebar buckling, which is the driving rebar fracture mechanism in columns of special moment resisting frames. Also, no fracture was observed in transverse reinforcements in all specimens.

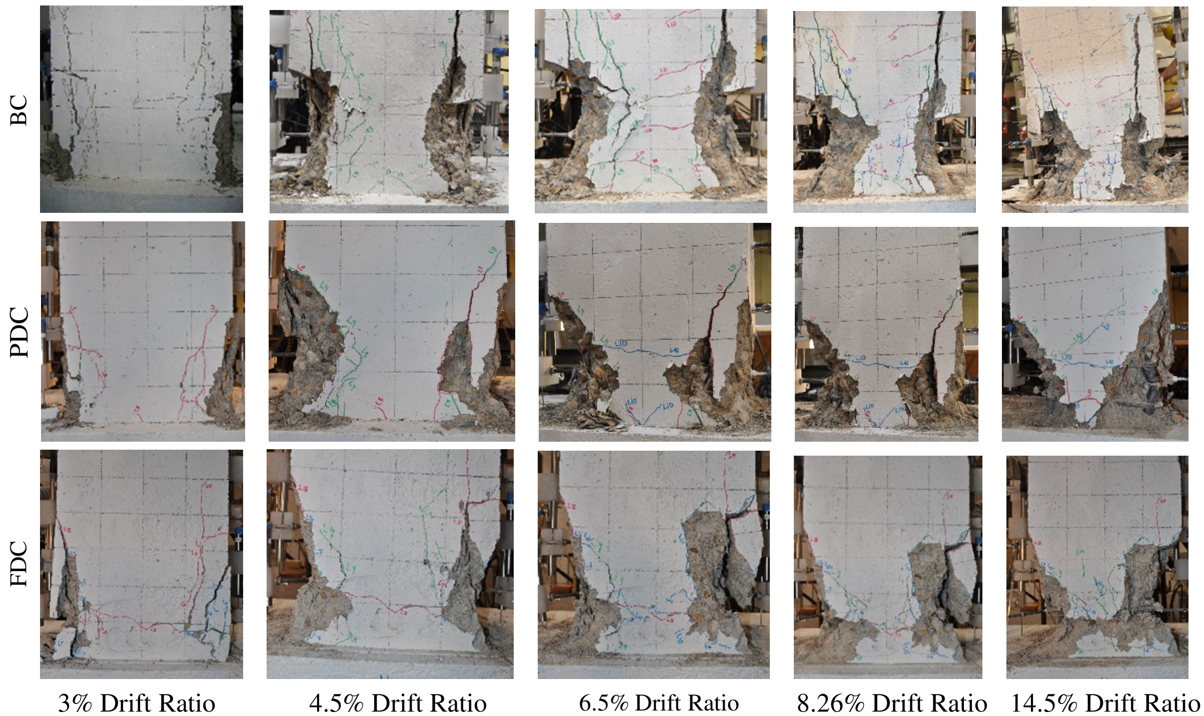

Fig. 6 – Concrete damage

Fig. 7 – Rebar fracture after extension

2.3.2. Curvature data

The curvature along the plastic hinge length (L_p) was calculated using the data from the curvature rod system. The rods were located at 3.5 in. [89 mm], 8.5 in. [216 mm], 13.5 in. [343 mm], 18.5 in. [470 mm], and 23.5 in. [597 mm] above the column-footing interface. Average curvature was calculated using Eq. (1) as below:

$$\varphi_i = \frac{\Delta\theta_i}{H_i} \tag{1}$$

where φ_i is the average curvature over the height monitored, H_i is the initial vertical distance between adjacent curvature rods, and $\Delta\theta_i$ is the relative rotation between two adjacent cross sections calculated using Eq. (2) as below:

$$\Delta\theta_i = \frac{\delta_{i,W} - \delta_{i,E}}{L_i} \quad (2)$$

where $\delta_{i,W}$ and $\delta_{i,E}$ are the displacements measured by the west and east LVDTs, respectively, and L_i is the horizontal distance measured between the west and east LVDTs.

Fig. 8 shows the average curvature of each specimen over the plastic hinge length measured by curvature rod system at different drift ratios. In specimen BC, as the drift ratio increases, concrete deformations increase and propagate along the column height over the plastic hinge length (L_p=23 in. [584 mm]). In contrast, consistent with the damage pattern (Fig. 6), in PDC and FDC specimens, concrete deformations are mostly concentrated at the column end over a length about 8 in. [203 mm] above the interface.

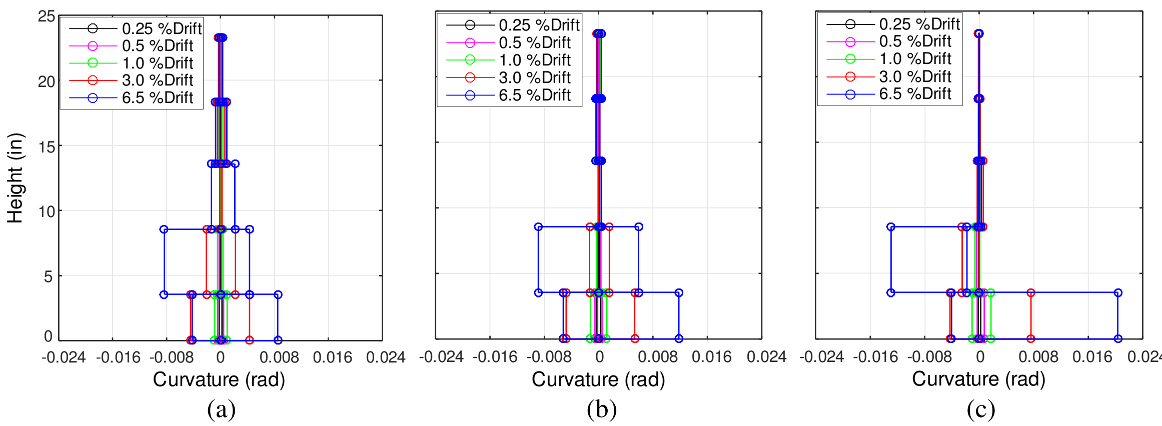

Fig. 8 – Average curvature over the plastic hinge length at various drift ratios: (a) BC; (b) PDC; (c) FDC (1 in. = 25.4 mm).

2.3.3. Strains in Steel Reinforcement

The axial strain distribution of two longitudinal bars, namely, Rebar-1 and Rebar-5 (Fig. 3(e)) at different drift ratios up to 2% is shown in Fig. 9. The strain profiles are shown for the two longitudinal rebars – Rebar-1 and -5 – with the maximum number of working strain gauges up to a drift ratio of 2%. For Rebar-1, strains are plotted at the column-to-footing interface and at 1.25 in. [31.75 mm], 3.25 in. [83 mm] and 8.25 in. [210 mm] above the interface. For Rebar-5, strains are plotted at the column-to-footing interface and at 1.25 in. [31.75 mm], 3.25 in. [83 mm], 13.25 in. [337 mm] and 18.25 in. [464 mm] above the interface. The nominal yield strain (0.2%) of the steel bars is indicated by the green dashed line. In both rebars, strain concentration is observed primarily near the column-footing interface of the BC specimen, while in PDC and FDC the strain is averaged out over the debonded length of the rebars. According to the strain profile in Rebar-5, the strain at the interface of the BC specimen builds up to about 1%, while it is about 0.3 and 0.4% in PDC and FDC specimens, respectively, and almost constant along the monitored length of the rebar.

For the longitudinal reinforcement, yielding initiated at drift ratios of 0.75%, 1%, and 1.2% for the BC (Rebar-1), PDC (Rebar-1), and FDC (Rebar-4) specimens, respectively. No yielding was observed in the transverse reinforcement in all specimens. The maximum observed strain in the transverse rebar was approximately 0.12 %, for all specimens, which was below the nominal steel yield strain of 0.2%.

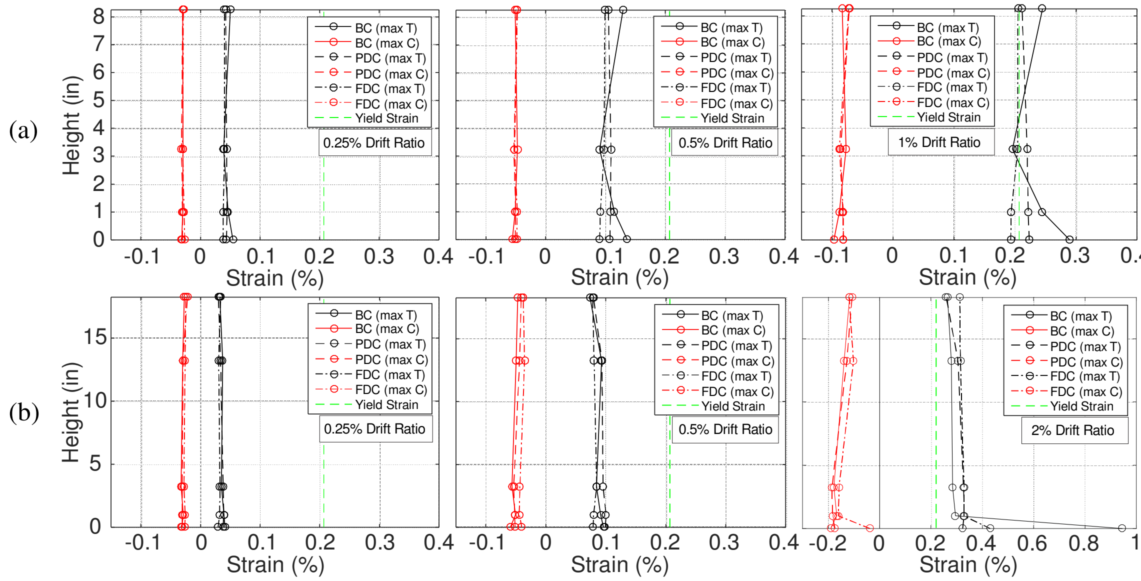

Fig. 9 – Axial strain profile in the height of: (a) Rebar-1; (b) Rebar-5 (1 in. = 25.4 mm).

3. Finite element modeling

Finite element modeling was performed using the general-purpose finite element software ABAQUS [12]. In the following sections the modeling assumptions and analysis results are described.

3.1. Model description

The BC column is modeled based on the dimensions of the experimental specimen shown in Fig. 1(a). The column and foundation are modeled using continuum three dimensional 8-noded solid element (C3D8R). Three dimensional 2-noded truss elements (T3D2) were used to model embedded longitudinal and transverse reinforcement bars. The embedded region constraint was used to connect reinforcement elements to the surrounding concrete. This option constrained the translational degrees of freedom of the nodes pf the embedded element (steel reinforcement) to the internal deformations of the hosting elements (concrete) at those locations. Mesh sensitivity analysis was conducted to determine a reasonable balance between solution accuracy and computation cost. Results of the analysis indicated that an element size less than 1.5 in. [38 mm] for the concrete and 1.0 in. [25.4 mm] for the steel reinforcement had no effect on the computed response. The bottom surface of the foundation was fixed as the boundary condition.

The concrete damaged plasticity model in ABAQUS [12] is used to model concrete material behavior. The definition of the concrete damaged plasticity model requires definition of plasticity parameters, as well as compressive and tensile response curves. The suggested default values from ABAQUS [12] are used for dilation angle (15°), eccentricity (0.1), uniaxial to biaxial stress ratio (1.16), stress variant (0.66), and viscosity parameter (0.0). The uniaxial compressive strength of concrete was considered to be 5 ksi [34.5 MPa]. Young's modulus and Poisson's ratio of concrete were assumed to be 3650 ksi [25166 MPa] and 0.2, respectively.

Longitudinal and transverse reinforcement behavior was defined as an elastic-plastic material using a bilinear curve. The nominal yield stress of steel reinforcement was considered to be 60 ksi [414 MPa]. Slope of the plastic range was assumed to be about 1.0 % of the steel modulus of elasticity.

In the first step of the analysis, the gravity load was applied as a uniform pressure to the top surface of the column. In the second analysis step, a linearly increasing lateral displacement was imposed to the top surface of the column up to 10% drift ratio.

3.2. Analysis results

A comparison of the predicted and measured damage for the BC column at various drift ratios is presented in Fig. 10. The experimentally observed damage, including crushing of the concrete and tensile cracking, is well captured by the finite element model. Moreover, the ABAQUS model predicted the propagation of damage over the cross-section depth and height of the column as was observed in the experiment.

Fig. 11 presents the predicted and measured force-drift ratio relationships of BC. There is good agreement between the predicted and experimentally measured cyclic response. It is noted that initial stiffness, peak strength and strength deterioration were captured reasonably well. However, small pinching at the end of the unloading branches – most probably resulting from bond-slip effects –at drift ratios larger than 3-4% was not captured.

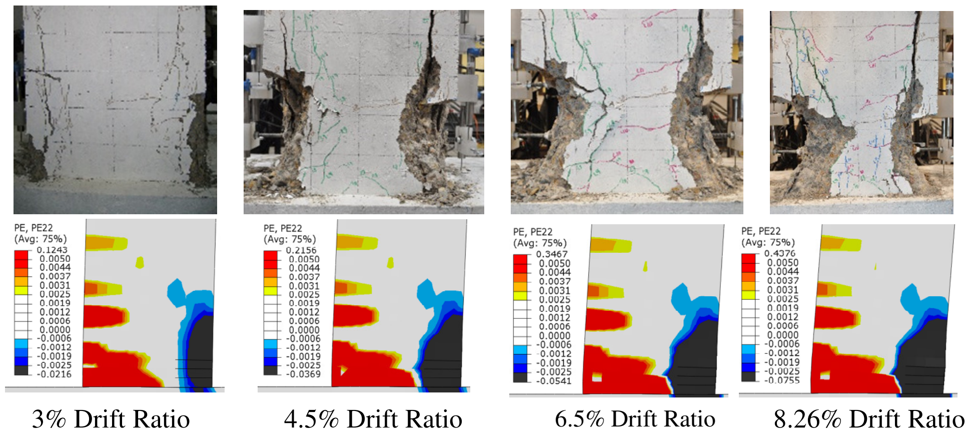

Fig. 10 – Predicted and measured damage to BC.

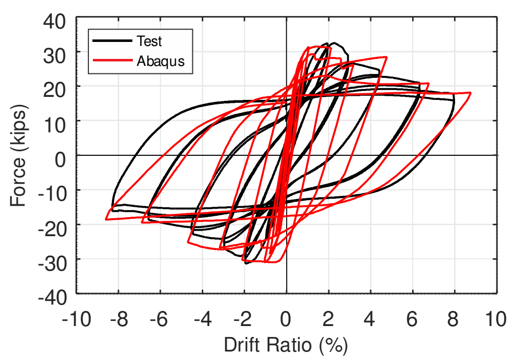

Fig. 11 – Predicted vs. measured lateral force vs. drift ratio for BC column (1 kip = 4.45 kN).

4. Conclusions

The objective of this study was to experimentally investigate the effect of debonding of the longitudinal reinforcement at the location of the plastic hinge on the performance of reinforced concrete (RC) columns in special moment resisting frames designed for seismic regions per ACI 318-11 [24]. The experimental program consisted of quasi-static cyclic testing of three nearly full-scale (~1:1.14) cantilever columns with 14 in. × 14 in. [356 mm × 356 mm] square cross-section and shear span-to-depth ratio of 5.5. The key outcomes of this study are:

- Debonding of the longitudinal reinforcement at the location of the plastic hinge resulted in early concrete cracking at the bottom of the columns and delayed yielding of the (debonded) longitudinal reinforcement. Yielding of the longitudinal reinforcement was first observed at a drift ratio of 0.75% for the column with the bonded reinforcement, and at 1% and 1.2% for the columns with the debonded reinforcement over half and full plastic hinge length, respectively.
- Reinforcement debonding decreased concrete damage spreading, because of the loss of strain compatibility between concrete and debonded reinforcement. For the column with the fully bonded reinforcement, concrete damage was observed over the entire (nominal) plastic hinge length, while

concrete damage spreading did not exceed half of the nominal plastic hinge length for the columns with the debonded reinforcement. Partial debonding changed the column deformation mechanism from flexure over the plastic hinge, for the column with bonded reinforcement, to rocking at the bottom, for columns with debonded reinforcement.

- The lateral stiffness and peak strength decreased with the debonded length, while softening (in the post peak branch of the hysteretic curve) increased with the debonded length. This response degradation was primarily controlled by local buckling of the longitudinal reinforcement, which led to low-cycle fatigue and eventual rebar fracture. Although, the selected debonding technique eliminated bonding stresses between concrete and steel reinforcement, it did not prevent rebar buckling, which, under the applied cyclic loading, led to slightly lower stiffness, strength and deformation capacity properties.
- The three-dimensional finite element model generated for the column provided prediction of the cyclic response that were in good agreement with the experimentally measured data. Such models can be used to further investigate the proposed concept and expand the findings of this research.

5. References

[1] Nakaki SD, Stanton JF, Sritharan S. An overview of the PRESSS five-story precast test building. PCI journal. 1999;44:26-39.
[2] Trono W, Jen G, Panagiotou M, Schoettler M, Ostertag CP. Seismic Response of a Damage-Resistant Recentering Posttensioned-HYFRC Bridge Column. Journal of Bridge Engineering. 2014.
[3] Pang JB, Eberhard MO, Stanton JF. Large-bar connection for precast bridge bents in seismic regions. Journal of Bridge Engineering. 2009;15:231-9.
[4] Ou YC, Tsai MS, Chang KC, Lee GC. Cyclic behavior of precast segmental concrete bridge columns with high performance or conventional steel reinforcing bars as energy dissipation bars. Earthquake Engineering & Structural Dynamics. 2010;39:1181-98.
[5] Kang S-M, Kim O-J, Park H-G. Cyclic loading test for emulative precast concrete walls with partially reduced rebar section. Engineering Structures. 2013;56:1645-57.
[6] Kawashima K, Hosoiri K, Shoji G, Sakai J-i. Effect of Unbonding of Main Reinforcements at Plastic Hinge Region for Enhancing Ductility of Reinforced Concrete Bridge Columns. Proceedings-Japan Society of Civil Engineers: DOTOKU GAKKAI; 2001. p. 45-64.
[7] Aviram A, Stojadinovic B, Parra-Montesinos GJ. High-performance fiber-reinforced concrete bridge columns under bidirectional cyclic loading. ACI Structural Journal. 2014;111.
[8] Pandey G, Mutsuyoshi H, Maki T. Seismic performance of bond controlled RC columns. Engineering Structures. 2008;30:2538-47.
[9] Pandey GR, Mutsuyoshi H. Seismic performance of reinforced concrete piers with bond-controlled reinforcements. ACI structural journal. 2005;102.
[10] Yu J, Tan KH. Special Detailing Techniques to Improve Structural Resistance against Progressive Collapse. Journal of Structural Engineering. 2013;140.
[11] Choi J-W, Ali M, Alexander SD. Behavior of slab-column connections with partially debonded reinforcement under lateral loading. Canadian Journal of Civil Engineering. 2009;36:463-72.
[12] SIMULIA. Abaqus analysis user's manual, Version 6.13. SIMULIA,The Dassault Systèmes, Realistic Simulation,USA; 2013.
[13] Filiatrault A, Tremblay R, Christopoulos C, Folz B, Pettinga D. Elements of Earthquake Engineering and Structural Dynamics. 3rd ed. Montreal, Canada: Presses Internationales Polytechnique; 2013.
[14] ASCE/SEI 7-10. Minimum Design Loads for Buildings and Others Structures. Reston, VA: American Society of Civil Engineers (ASCE); 2010.
[15] ACI 318-11. Building Code Requirements for Structural Concrete and Commentary. 38800 Country Club Drive, Farmington Hills, MI 48331 U.S.A.: American Concrete Institute; 2011.